



# Sodiophilicity/potassiophilicity chemistry in sodium/potassium metal anodes

Xiang Chen<sup>a,1</sup>, Yun-Ke Bai<sup>a,1</sup>, Xin Shen<sup>a</sup>, Hong-Jie Peng<sup>b</sup>, Qiang Zhang<sup>a,\*</sup>

<sup>a</sup> Beijing Key Laboratory of Green Chemical Reaction Engineering and Technology, Department of Chemical Engineering, Tsinghua University, Beijing 100084, China

<sup>b</sup> Department of Chemical Engineering, Stanford University, Stanford, CA 94305, USA

## ARTICLE INFO

### Article history:

Received 6 March 2020

Revised 27 March 2020

Accepted 27 March 2020

Available online 13 April 2020

### Keywords:

Sodium and potassium metal anodes

Sodiophilicity and potassiophilicity

Carbon materials

First-principles calculations

Dendrite-free electrode

## ABSTRACT

Heteroatom-doped carbon materials have been widely used as sodium (Na) and potassium (K) metal anode frameworks to achieve uniform Na and K depositions. If the origin of the Sodiophilicity and potassiophilicity of doping sites in heteroatom-doped carbon host are clearly understood, the nucleation and growth behavior of Na and K can be precisely regulated in working batteries. Herein the Sodiophilicity and potassiophilicity chemistries of carbon materials are probed through first-principles calculations. The local dipole of doping functional groups and charge transfer during Na/K deposition are regarded as key principles to reveal the sodiophilic and potassiophilic nature of doping sites. Especially, O–B, O–S, and O–P co-doping strategy are predicted to be effective methods to improve the Sodiophilicity and potassiophilicity of carbon hosts and thus render safe and dendrite-free Na and K metal anodes. This work affords a deep and insightful understanding of Sodiophilicity and potassiophilicity chemistry of Na and K anodes and establishes general principles of designing highly sodiophilic and potassiophilic carbon frameworks.

© 2020 Science Press and Dalian Institute of Chemical Physics, Chinese Academy of Sciences. Published by Elsevier B.V. and Science Press. All rights reserved.

## 1. Introduction

Alkali metal batteries are strongly considered as promising next-generation energy storage systems due to their larger energy density compared with routine rocking-chair batteries [1–4]. Especially, lithium (Li) metal anodes have both a very high specific capacity of 3810 mAh g<sup>-1</sup> and an extremely low electrochemical potential (−3.040 V vs. the standard hydrogen electrode), affording Li metal batteries outstanding advantages in electric vehicle and portable device applications [5–10]. However, the issue of the limited resource and the high cost of lithium element resists the applications of Li metal batteries in large-scale practical energy storage. Sodium (Na) and potassium (K) are expected to be a more abundant, cost-effective, and sustainable alternative to Li as anode materials in these applications [11–15]. Therefore, Na and K metal batteries have been strongly considered widely.

Similar with Li metal anodes, Na and K metal anodes are also faced with disastrous dendrite growth issues [11,12,16]. The higher reactivity of Na and K metal can cause more serious side reactions

with electrolytes and thus induce a smaller Coulombic efficiency and even more serious safety hazards comparing with Li metal. Several strategies have been proposed to address the issues of Na/K dendrite growth, including the anode framework construction to deliver a uniform deposition [17–22], the electrolyte regulation to achieve a stable anode–electrolyte interface [23–26], and the adoption of solid-state electrolytes [27–31]. Among these strategies, the construction of sodiophilic and potassiophilic frameworks can resist infinite relative volume expansion and the growth of dendrites and simultaneously. Therefore, many frameworks, especially various carbon materials, have been delicately designed to achieve a stable and non-dendritic anode. For example, three-dimensional copper was reported to achieve both dendrite-free Na and K metal anodes [18,22]. Yang and co-authors [20] adopted an aligned carbon nanotube membrane as the anode framework, in which K has a good wettability and can be spatially distributed. As results, the composite anode shows stable plating/stripping profiles with a low polarization and non-dendritic deposition morphology. Huang and coworkers [32] reported nitrogen- and sulfur-doped hollow carbon fibers as sodium metal anode hosts. The large specific surface area and sodiophilic functional groups of the carbon host contribute to a dissipated local current density and a homogenous plating morphology.

\* Corresponding author.

E-mail address: [zhang-qiang@mails.tsinghua.edu.cn](mailto:zhang-qiang@mails.tsinghua.edu.cn) (Q. Zhang).

<sup>1</sup> These authors contributed equally to this work.

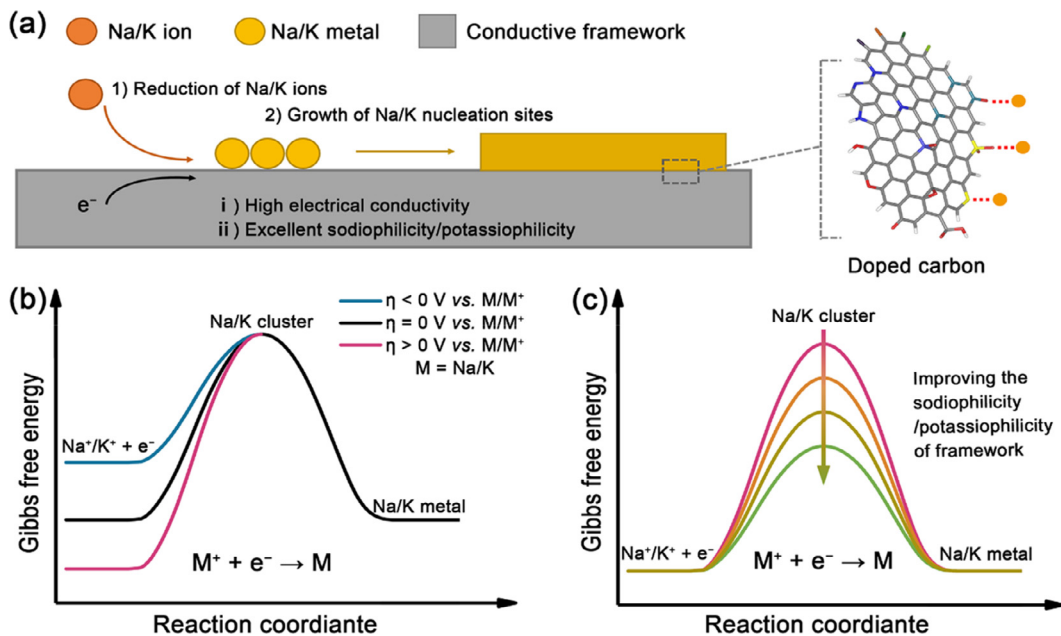


**Fig. 1.** Schematic of sodiophilicity and potassiophilicity. (a) The deposition of Na/K ions on carbon hosts. (b) The Gibbs free energy change as Na/K ion deposition at different potentials. (c) The role of sodiophilicity and potassiophilicity in regulating Na/K ion nucleation barrier on anode framework.

Among various framework materials, carbon materials are widely applied because of their high electrical conductivity, low expanse, and easy fabrication [17,20,32–35]. What is more, heteroatom-doping strategy can improve the practical performance of carbon-host anodes and resist the growth of Na/K dendrites, which is also an effective strategy in Li metal anodes [36–42]. However, a fundamental understanding of the role of heteroatom-doping in regulating Na/K deposition is still lacking. If a deep and fundamental understanding of sodiophilicity and potassiophilicity chemistries of carbon materials can be built, a delicate carbon host can be rationally designed for Na/K metal anodes to achieve dendrite-free growth and thus render stable Na/K metal batteries.

In this contribution, the sodiophilicity and potassiophilicity chemistries of carbon materials are probed through first-principles calculations. The local dipole and charge transfer are confirmed as key principles for designing highly sodiophilic and potassiophilic carbon hosts. The O-doping and O-B co-doping are predicted to be the best mono-doping and co-doping strategies, respectively. This work reveals the sodiophilicity and potassiophilicity chemistries for Na/K metal anodes at the atomic level and affords rational strategies for designing highly sodiophilic and potassiophilic carbon hosts.

## 2. Results and discussion

The Na/K ions in electrolytes are coordinated with solvents or anions from salts. The Na/K ions can interact with anode frameworks or solid-electrolyte interphase (SEI) and lose the interaction with solvents or anions from electrolytes simultaneously, which is known as desolvation (Fig. 1(a)). When the electrode potential ( $\eta$ ) is reduced to below zero (versus M/M<sup>+</sup>, M = Na or K), the Na<sup>+</sup>/K<sup>+</sup> will have a higher energy than Na/K metal (Fig. 1(b)). Then the Na/K ions are reduced at the nucleation sites due to the charge transfer from the metal anode. The nucleation sites are expected to have a high electrical conductivity and excellent sodiophilicity/potassiophilicity. The former can ensure effective charge transfer from anodes to the absorbed ions. The latter is the key to reduce the nucleation barrier during Na/K depositions

(Fig. 1(c)). When the sodiophilicity/potassiophilicity is improved, the absorbed Na/K can form a strong interaction with the working hosts and its energy level is reduced, thus rendering a very small nucleation barrier. Therefore, rationally designing highly sodiophilic/potassiophilic hosts is necessary to achieve a low nucleation barrier and thus a uniform deposition, in which the interaction between deposited Na/K and carbon hosts plays a critical role.

In order to probe the sodiophilicity/potassiophilicity of carbon hosts, the graphene nanoribbons (GNRs) were built (Fig. S1). A series of B-, N-, O-, F-, P-, S-, Cl-, Br-, and I-doping was further considered. Specifically, the B-doping includes graphitic boron in the bulk phase (bgB), graphitic boron on the edge (egB), and B-2C-O-type boron (oB). The N-doping includes quaternary nitrogen in the bulk phase (bqN), quaternary nitrogen on the edge (eqN), pyrrolic nitrogen (rN), and pyridinic nitrogen (pN). The O-doping includes carboxylic group (aO), cyclic oxygen (cO), epoxy group (eO), hydroxyl group (hO), and ketone group (kO). The S-doping includes sulfur (S) and sulfonyl group (oS). The other doping only considers one functional group. As defect is often induced as doping, three typical defects, five-carbon rings (C5), seven-carbon rings (C7), and five-carbon rings adjacent to seven-carbon rings (C5 + C7), are also considered. Besides, the influence of the number of graphene layer is also investigated. For each model, Na and K atoms are allowed to interact with the doping site to estimate its sodiophilicity/potassiophilicity. The sodiophilic/potassiophilic sites are expected to induce a large binding energy with the absorbed Na/K species.

The binding energies of Na/K on pristine and heteroatom-doped carbon materials are summarized in Fig. 2 and the optimized geometrical structures are presented in Figs. S2 and S3. In overall, Na and K share a similar binding energy trend. The aO-doping exhibits the largest binding among mono-doping cases, -2.03 and -2.27 eV for both Na and K absorption, respectively. In composition, the binding energies on pristine graphene are only -1.17 and -1.59 eV for Na and K, respectively. An increased binding energy can reduce the nucleation overpotential according to the lithiophilicity theory [36]. Besides aO-doping, bgB-, egB-, pN-, eO-, and kO-doping also

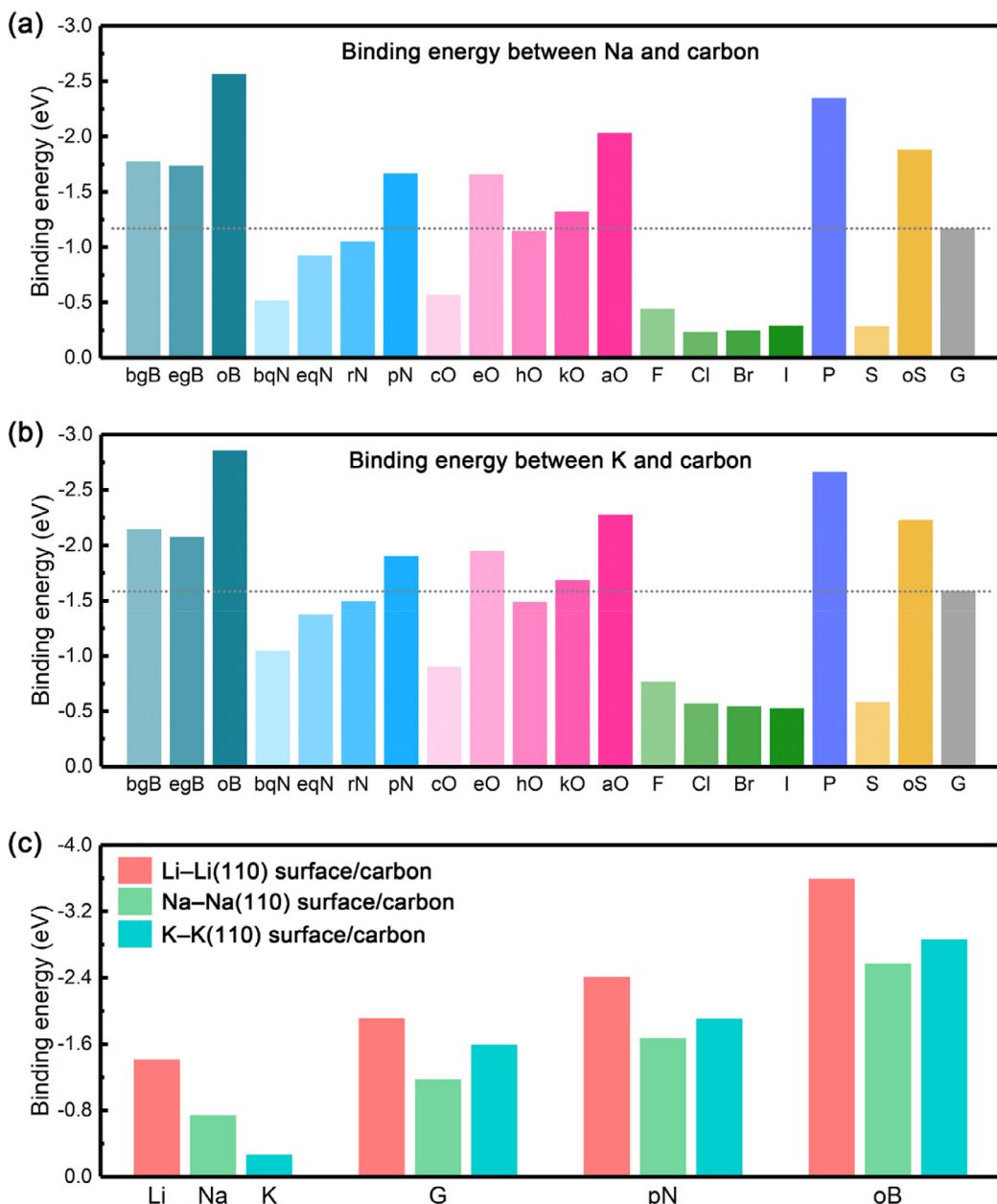


**Fig. 2.** The summary of binding energy on carbon materials. (a) The binding energy between Na and carbon. (b) The binding energy between K and carbon. (c) The comparison of the binding energy of Li/Na/K on carbon or Li/Na/K(110) surfaces.

delivers a larger binding energy than pristine graphene, indicating promising doping choices for practical design of three-dimensional carbon hosts. Beyond mono-doping, co-doping strategy can even achieve larger binding energies. For example, oB- and P-doping can deliver binding energies of -2.57 and -2.35 eV for Na adsorption respectively, and -2.86 and -2.67 eV for K adsorption respectively.

Similar with heteroatom-doping, defects in carbon can also regulate the interaction towards Na/K atoms (Figs. S4 and S5). The C7 and C5 + C7 defects deliver a similar binding energy, comparing with pristine graphene. The C5 defect can increase the binding energy significantly, -1.83 and -2.21 eV for Na and K adsorption, respectively. But this enhancement is less obvious than aO-, oB-, P-, and oS-doping. Different from defects, the number of graphene layers has a very small influence on the binding energy (Figs. S6–S8). One, two, and three-layered graphene models (pristine or with

bqN/bgB/P-decoration) are considered. For example, the energy difference is within 0.11 and 0.10 eV for Na and K adsorption on pristine graphene, respectively.

Compared with Li adsorption on doped-carbon, Na and K have several differences. Firstly, Li can be stable above the five-atom ring of rN site [36]. While Na and K cannot be stabilized there and will move to the adjacent six-carbon ring site (Figs. S2h and S3h), which is induced by the larger ionic radius of  $\text{Na}^+$  and  $\text{K}^+$ , comparing with  $\text{Li}^+$ . Secondly,  $\text{Li}^+$  can break the C-O bond in eO functional group and the I-C bond in I-doping case while  $\text{Na}^+$  and  $\text{K}^+$  are stable with eO and I functional groups (Figs. S2k, S2t, S3k, and S3t) [36]. The stronger interaction between adsorbed species and carbon make it easier to destroy the primitive structure. Thirdly, Li, Na, and K have different binding energy trends in carbon materials and metal surface. Specifically, the binding energy in all doping cases follows as Li > K > Na (Fig. 2(c)). This is consistent with

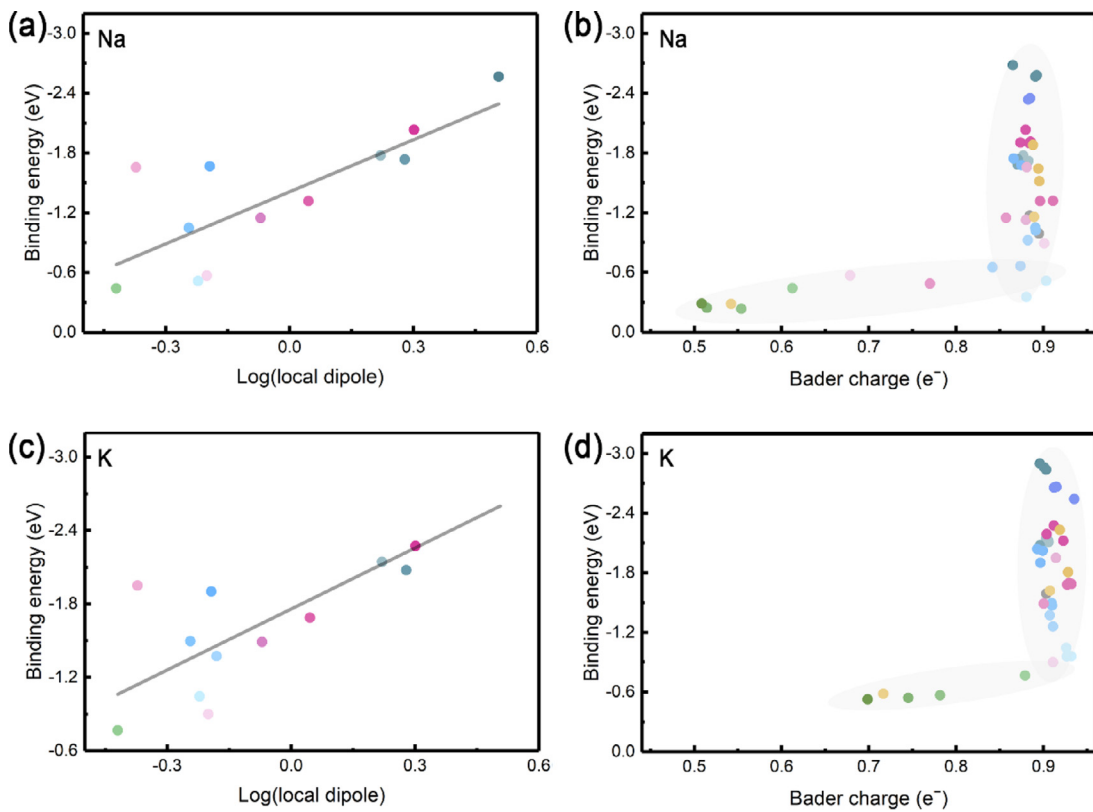


**Fig. 3.** The principles of designing sodiophilic/potassiophilic Na/K frameworks. The correlation between Na atom binding energy and (a) Log(local dipole) and (b) charge transfer. The correlation between K atom binding energy and (c) Log(local dipole) and (d) charge transfer.

fact that only Li and K can be intercalated into graphite layers as Na forms a weak interaction with the carbon layer [43]. However, the binding energy on Li/Na/K on each (110) surface is ordered as Li > Na > K (Fig. 2(c)). Among Li, Na, and K elements, K has the largest atomic radius and forms the weakest metallic bond. Therefore, K is supposed to deliver the lowest binding energy on metal surface.

In order to compare the differences between various doping and explore general principles for designing highly sodiophilic/potassiophilic carbon hosts, the binding energy is correlated with the local dipole of doping site and charge transfer during adsorption, respectively (Fig. 3). Although the electronegativity can differ various doping elements, it cannot explain the significant change between different functional groups of a same doping element. Therefore, the local dipole, which is defined as the dipole between the doping atom and its adjacent atom, is proposed herein. The doping site with a large local dipole is supposed to form a large ion-dipole interaction toward Na/K ions and thus a large binding energy and a small nucleation barrier. Besides, a doping atom with a large electronegativity can induce a large charge transfer and thus a large local dipole to some degree. Therefore, the influence of elemental electronegativity is included in the concept of local dipole but the latter can describe the local environment of doping sites better, which is supposed to determine the binding energy directly. As expected, a larger local dipole can deliver a larger binding energy with both Na and K atoms (Fig. 3(a) and (c)), which also explains the origin of the high sodiophilicity/potassiophilicity of co-doping sites. For instance, the oB-doping site has the largest local dipole of  $3.21 \text{ e}^- \text{ Å}$  [36] and thus the largest binding energy towards Na and K atom,  $-2.57$  and  $-2.86$  eV, respectively.

Besides local dipole, the charge transfer during Na/K adsorption is correlated with the binding energy (Fig. 3(b) and (d)). A key value of charge transfer of  $0.85$  and  $0.89 \text{ e}^-$  is found for Na and K, respectively. Below the key value, the binding energy is pretty small, indicating bad sodiophilicity and potassiophilicity. While the binding energy is spread when the charge transfer is above the key value. Therefore, an efficient charge transfer is very essential for achieving high sodiophilic and potassiophilic framework. Comparing with Na, K have a smaller electronegativity and is easier to lose electrons. Therefore, the key value of K is larger than Li.

The Bader charge and differential charge density analyses are further conducted to reveal the charge transfer during Na/K nucleation on doping sites (Fig. 4). There is an obvious charge transfer from the Na/K atom to pN- and aO-dopant (Fig. 4(d), (e), (g), and (h)), indicating a strong chemical interaction. While the charge transfer is less significant in the case of F-doping, especially for Na-adsorption. Specifically, the absorbed Na atom loses  $0.87$ ,  $0.88$ , and  $0.61 \text{ e}^-$  on pN-, aO-, and F-doping sites, respectively. The absorbed K atom loses  $0.90$ ,  $0.91$ , and  $0.88 \text{ e}^-$  on pN-, aO-, and F-doping sites, respectively. The difference among N-, O-, and F-doping can be explained by their electronic structures. The N, O, and F atoms all form  $\sigma$ -bonds with the adjacent carbon atom and withdraw electrons from the carbon atom due to a larger electronegativity than carbon. Besides, both N and O atoms can take part in the delocalized  $\pi$  system of graphene, which further increases their negative charge state. However, in the case of F-doping, the fully filled  $p$  orbitals of F atom form a  $p-\pi$  conjunction with the GNR plane that feedbacks electrons from the fluorine to carbon. Therefore, the F atom is less electronegative than N and O atoms, confirmed by the Bader charge analyses (Fig. 4(a)–(c)). Compared with Na, K has a smaller electronegativity and is easier

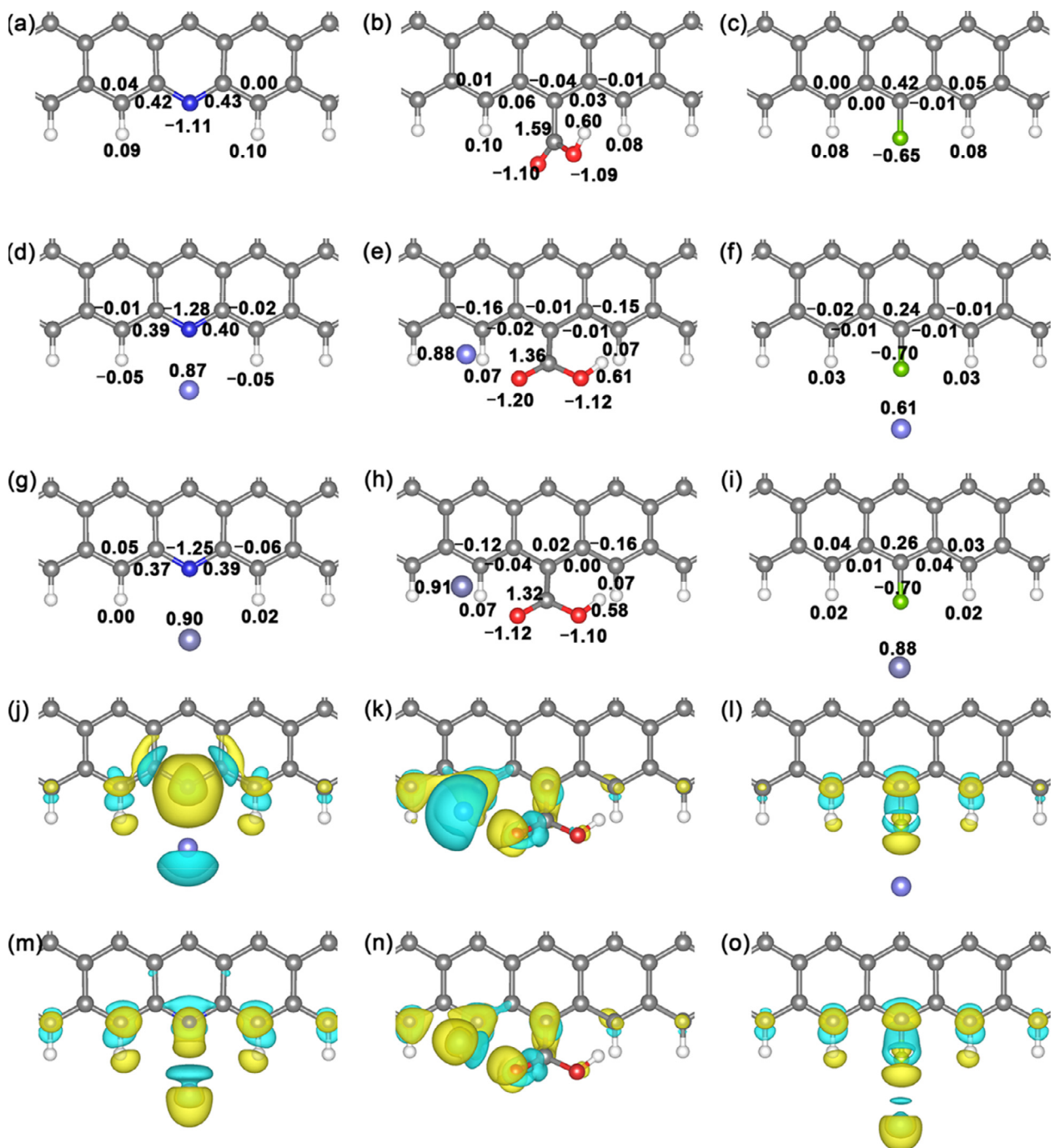


**Fig. 4.** The Bader charge and differential charge analyses. The Bader charge distribution (a) pN-, (b) aO-, and (c) F-GNRs. The Bader charge distribution of Na adsorption on (d) pN-, (e) aO-, and (f) F-GNRs. The Bader charge distribution of K adsorption on (g) pN-, (h) aO-, and (i) F-GNRs. The differential charge density of Na adsorption on (j) pN-, (k) aO-, and (l) F-GNRs. The differential charge density of K adsorption site on (m) pN-, (n) aO-, and (o) F-GNRs. The yellow and cyan surfaces correspond the charge gain and lost regions, respectively (isovalue, 0.0025). The hydrogen, carbon, nitrogen, oxygen, fluorine, sodium, and potassium atoms are marked as white, gray, blue, red, cyan, light blue, and blue-gray, respectively.

transfer electrons to carbon plane. These results also agree with the charge analyses of the lithiophilicity of doped-carbon material [36].

### 3. Conclusions

The sodiophilicity and potassiophilicity of doped-carbon materials are proposed. The aO-doping and oB-doping are predicted to be best doping strategy for mono- and co-doping cases, respectively. The important role of the local dipole of doping site

and the electron transfer during Na/K nucleation is highlighted. This work reveals the nature of sodiophilicity and potassiophilicity chemistries in doped carbon materials and affords rational strategies for designing highly sodiophilic/potassiophilic carbon frameworks for Na/K metal anodes.

### Declaration of Competing Interest

The authors declare that they have no competing interests.

## Acknowledgments

This work was supported by the National Key Research and Development Program (2016YFA0202500), the National Natural Science Foundation of China (21825501), and the Tsinghua University Initiative Scientific Research Program. The authors acknowledged the support from Tsinghua National Laboratory for Information Science and Technology for theoretical simulations. We thank Hao-Ran Li, Rui Zhang, and Xin-Bing Cheng for helpful discussions.

## Supplementary materials

Supplementary material associated with this article can be found, in the online version, at doi:10.1016/j.jecchem.2020.03.051.

## References

- [1] H.J. Peng, J.Q. Huang, Q. Zhang, Chem. Soc. Rev. 46 (2017) 5237–5288.
- [2] H. Wang, D. Yu, C. Kuang, L. Cheng, W. Li, X. Feng, Z. Zhang, X. Zhang, Y. Zhang, Chem 5 (2019) 313–338.
- [3] J. Xiang, L. Yang, L. Yuan, K. Yuan, Y. Zhang, Y. Huang, J. Lin, F. Pan, Y. Huang, Joule 3 (2019) 2334–2363.
- [4] H. Liu, X.-B. Cheng, Z. Jin, R. Zhang, G. Wang, L.-Q. Chen, Q.-B. Liu, J.-Q. Huang, Q. Zhang, Energy Chem. 1 (2019) 100003.
- [5] X.-B. Cheng, R. Zhang, C.-Z. Zhao, Q. Zhang, Chem. Rev. 117 (2017) 10403–10473.
- [6] D. Lin, Y. Liu, Y. Cui, Nat. Nanotechnol. 12 (2017) 194–206.
- [7] R. Wang, W. Cui, F. Chu, F. Wu, J. Energy Chem. 48 (2020) 145–159.
- [8] X. Zhang, A. Wang, X. Liu, J. Luo, Accounts Chem. Res. 52 (2019) 3223–3232.
- [9] X.-Q. Zhang, C.-Z. Zhao, J.-Q. Huang, Q. Zhang, Engineering 4 (2018) 831–847.
- [10] R. Xu, X.-B. Cheng, C. Yan, X.-Q. Zhang, Y. Xiao, C.-Z. Zhao, J.-Q. Huang, Q. Zhang, Matter 1 (2019) 317–344.
- [11] J.-Y. Hwang, S.-T. Myung, Y.-K. Sun, Adv. Funct. Mater. 28 (2018) 1802938.
- [12] B. Lee, E. Paek, D. Mitlin, S.W. Lee, Chem. Rev. 119 (2019) 5416–5460.
- [13] Y. Zhao, K.R. Adair, X. Sun, Energy Environ. Sci. 11 (2018) 2673–2695.
- [14] C. Zhao, Y. Lu, J. Yue, D. Pan, Y. Qi, Y.-S. Hu, L. Chen, J. Energy Chem. 27 (2018) 1584–1596.
- [15] Y. Liang, C.-Z. Zhao, H. Yuan, Y. Chen, W. Zhang, J.-Q. Huang, D. Yu, Y. Liu, M.-M. Titirici, Y.-L. Chueh, H. Yu, Q. Zhang, InfoMat 1 (2019) 6–32.
- [16] B. Thirumalraj, T.T. Hagos, C.-J. Huang, M.A. Teshager, J.-H. Cheng, W.-N. Su, B.-J. Hwang, J. Am. Chem. Soc. 141 (2019) 18612–18623.
- [17] S. Bing, L. Peng, Z. Jinjiang, W. Dan, M. Paul, W. Chengyin, N.P.H. L, W. Guoxiu, Adv. Mater. 30 (2018) 1801334.
- [18] P. Liu, Y. Wang, Q. Gu, J. Nanda, J. Watt, D. Mitlin, Adv. Mater. 32 (2020) 1906735.
- [19] J. Luo, C. Wang, H. Wang, X. Hu, E. Matios, X. Lu, W. Zhang, X. Tao, W. Li, Adv. Funct. Mater. 29 (2019) 1805946.
- [20] L. Qin, Y. Lei, H. Wang, J. Dong, Y. Wu, D. Zhai, F. Kang, Y. Tao, Q.-H. Yang, Adv. Energy Mater. 9 (2019) 1901427.
- [21] X. Tang, D. Zhou, P. Li, X. Guo, B. Sun, H. Liu, K. Yan, Y. Gogotsi, G. Wang, Adv. Mater. 32 (2020) 1906739.
- [22] T.-S. Wang, Y. Liu, Y.-X. Lu, Y.-S. Hu, L.-Z. Fan, Energy Storage Mater. 15 (2018) 274–281.
- [23] S. Choudhury, S. Wei, Y. Ozhabes, D. Gunceler, M.J. Zachman, Z. Tu, J.H. Shin, P. Nath, A. Agrawal, L.F. Kourkoutis, T.A. Arias, L.A. Archer, Nat. Commun. 8 (2017) 898.
- [24] L. Gao, J. Chen, Y. Liu, Y. Yamauchi, Z. Huang, X. Kong, J. Mater. Chem. A 6 (2018) 12012–12017.
- [25] L. Guo, H. Wang, D. Yu, X. Wang, Z. Niu, M. Chen, L. Cheng, W. Zhou, Angew. Chem. Int. Ed. 58 (2019) 16451–16455.
- [26] Z. Xu, J. Yang, T. Zhang, L. Sun, Y. Nuli, J. Wang, S.-i. Hirano, Adv. Funct. Mater. 29 (2019) 1901924.
- [27] H. Gao, S. Xin, L. Xue, J.B. Goodenough, Chem 4 (2018) 833–844.
- [28] H. Yuan, H. Li, T. Zhang, G. Li, T. He, F. Du, S. Feng, J. Mater. Chem. A 6 (2018) 8413–8418.
- [29] C. Zhao, L. Liu, Y. Lu, M. Wagemaker, L. Chen, Y.-S. Hu, Angew. Chem. Int. Ed. 58 (2019) 17026–17032.
- [30] X. Xu, Y. Li, J. Cheng, G. Hou, X. Nie, Q. Ai, L. Dai, J. Feng, L. Ci, J. Energy Chem. 41 (2020) 73–78.
- [31] H. Jia, L. Peng, Z. Zhang, T. An, J. Xie, J. Energy Chem. 48 (2020) 102–106.
- [32] X. Zheng, P. Li, Z. Cao, W. Luo, F. Sun, Z. Wang, B. Ding, G. Wang, Y. Huang, Small 15 (2019) 1902688.
- [33] L. Jiang, X.-B. Cheng, H.-J. Peng, J.-Q. Huang, Q. Zhang, eTransportation 2 (2019) 100033.
- [34] S.-S. Chi, X.-G. Qi, Y.-S. Hu, L.-Z. Fan, Adv. Energy Mater. 8 (2018) 1702764.
- [35] C. Chu, N. Wang, L. Li, L. Lin, F. Tian, Y. Li, J. Yang, S.-x. Dou, Y. Qian, Energy Storage Mater. 23 (2019) 137–143.
- [36] X. Chen, X.-R. Chen, T.-Z. Hou, B.-Q. Li, X.-B. Cheng, R. Zhang, Q. Zhang, Sci. Adv. 5 (2019) eaau7728.
- [37] R. Zhang, X.R. Chen, X. Chen, X.B. Cheng, X.Q. Zhang, C. Yan, Q. Zhang, Angew. Chem. Int. Ed. 56 (2017) 7764–7768.
- [38] B.-Q. Li, X.-R. Chen, X. Chen, C.-X. Zhao, R. Zhang, X.-B. Cheng, Q. Zhang, Research 2019 (2019) 4608940.
- [39] L. Huo, F. Su, Z. Yi, G. Cui, C. Zhang, N. Dong, C. Chen, P. Han, J. Electrochem. Soc. 166 (2019) A1603–A1610.
- [40] L. Ye, M. Liao, T. Zhao, H. Sun, Y. Zhao, X. Sun, B. Wang, H. Peng, Angew. Chem. Int. Ed. 58 (2019) 17054–17060.
- [41] L. Liu, Y.-X. Yin, J.-Y. Li, S.-H. Wang, Y.-G. Guo, L.-J. Wan, Adv. Mater. 30 (2018) 1706216.
- [42] H. Wu, Y. Zhang, Y. Deng, Z. Huang, C. Zhang, Y.-B. He, W. Lv, Q.-H. Yang, Sci. China Mater. 62 (2019) 87–94.
- [43] Y. Li, Y. Lu, P. Adelhelm, M.-M. Titirici, Y.-S. Hu, Chem. Soc. Rev. 48 (2019) 4655–4687.